

DYNAMICS OF INTERFACES IN THE TWO-DIMENSIONAL WAVE-PINNING MODEL

SHUNSUKE KOBAYASHI*, KOYA SAKAKIBARA†, AND TAIKEI UECHI‡

Abstract. We study the mass-conserved reaction-diffusion system known as the wave-pinning model, which serves as a minimal framework for describing cell polarity. In this model, the interplay between reaction kinetics and slow diffusion forms a sharp interface that partitions the domain into high- and low-concentration regions. We perform a detailed asymptotic analysis and derive higher-order approximation equations governing the motion of this interface. Our results show that on a fast timescale, the interface evolves via propagating front dynamics, whereas on a slow timescale, it evolves as an area-preserving mean curvature flow. Furthermore, using the derived free boundary problem, we demonstrate that on a significantly slower timescale, an interface whose endpoints lie on the domain boundary drifts along the boundary toward regions of higher curvature. In summary, our analysis reveals that the interface dynamics in the wave-pinning model exhibit a hierarchy of three distinct timescales: wave propagation on a fast timescale, curvature-driven area-preserving evolution on a slow timescale, and motion along the boundary on a significantly slower timescale.

Key words. dynamics of interfaces, matched asymptotic expansions, multiple timescale behavior, reaction-diffusion system

AMS subject classifications. 35C20, 35K57, 92C37

1. Introduction. Cell polarity, characterized by the asymmetric distribution of cellular components, plays a fundamental role in a wide range of biological processes including cell migration, division, and morphogenesis [5, 6, 10, 36]. At the same time, its disruption is a hallmark of many pathological conditions such as cancer [6, 24, 36]. Consequently, elucidating the mechanisms by which cells break symmetry remains a central challenge in modern biology. In parallel with this biological inquiry, symmetry breaking has long been a subject of intensive mathematical research. In this context, cell polarity has served as an intriguing case study, leading to the proposal of numerous mathematical models [4, 17, 20, 27, 30]. These studies have provided theoretical insights into how cells establish polarity and continue to drive research in mathematical biology (see, e.g., the reviews [12, 19, 23]).

In this paper, we study the wave-pinning model, which has emerged as a minimal and analytically tractable framework for explaining how cells achieve polarity [27, 28]. Biologically, this model captures the dynamics of Rho GTPases, which cycle between active membrane-bound and inactive cytosolic forms. These dynamics are distilled into a mass-conserved reaction-diffusion system on a bounded domain $\Omega \subset \mathbb{R}^2$:

$$\begin{aligned} (1.1a) \quad & \varepsilon \partial_t u = \varepsilon^2 \Delta u + f(u, v), & \text{in } \Omega \times (0, \infty), \\ (1.1b) \quad & \varepsilon \partial_t v = D \Delta v - f(u, v), & \text{in } \Omega \times (0, \infty), \\ (1.1c) \quad & \partial_\nu u = \partial_\nu v = 0, & \text{on } \partial\Omega \times (0, \infty), \end{aligned}$$

where $\varepsilon > 0$ is a sufficiently small parameter, $D > 0$ is a constant, and ν is the outward unit normal vector to the boundary $\partial\Omega$. The functions u and v represent the concentrations of the active and inactive forms, respectively. Detailed assumptions for

*Faculty of Engineering, University of Miyazaki, 1-1 Gakuen Kibanadainishi, Miyazaki 889-2192, Japan

†Faculty of Mathematics and Physics, Institute of Science and Engineering, Kanazawa University, Kakuma-machi, Kanazawa-shi, Ishikawa 920-1192, Japan

‡Division of Mathematical and Physical Sciences, Graduate School of Natural Science and Technology, Kanazawa University, Kakuma-machi, Kanazawa-shi, Ishikawa 920-1192, Japan

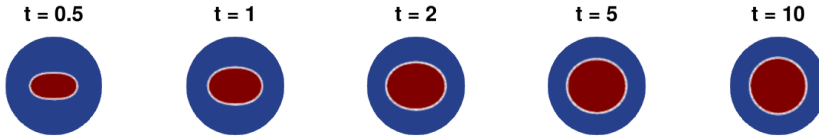


FIG. 1.1. *Numerical simulation of (1.1c) demonstrating the area-preserving, curvature-driven evolution on a slow timescale.*

this model are given in Section 2. The generation of polarity in this framework hinges on three essential properties: (i) a large disparity in diffusion coefficients ($\varepsilon^2 \ll D$), reflecting the rapid diffusion of cytosolic proteins; (ii) reaction kinetics $f(u, v)$ that are bistable with respect to u , allowing the coexistence of high and low states of u ; and (iii) the conservation of total mass. To understand the mechanism intuitively, imagine a local increase in the active form u . This initiates a wave of activation that propagates across the domain. However, since the total mass is conserved, the expansion of the high- u region rapidly depletes the available inactive form v . As the level of v drops below a critical level, the wave speed stalls, “pinning” the interface in place. This self-limiting growth is the essence of the wave-pinning mechanism. To elucidate the detailed dynamics of this wave-pinning process, formal asymptotic analysis has been employed to characterize the front behavior as ε tends to 0 [28]. Complementing these formal results, Gomez, Lam, and Mori rigorously demonstrated that the front solution to the shadow wave-pinning system converges to this sharp interface limit [18]. Beyond these fundamental analyses, the model has been extended to incorporate various biological factors, such as source and sink terms [35], feedback from F-actin [21], mechanical tension [37], and bulk-surface coupling [11, 16, 31]. In addition, the model has been applied to studies of cell motility [8, 9].

Here, we focus on the detailed dynamics of the interface after the initial front formation. The interface equations derived in previous studies, such as [28] and [18], correspond to leading-order approximations that are independent of the interfacial mean curvature. As noted by [18], these approximations can exhibit finite-time singularities, underscoring the necessity for deriving more accurate, higher-order interface equations. Incorporating such higher-order corrections is expected to regularize the dynamics and reveal that the interface evolves on a slow timescale analogously to volume-preserving mean curvature flow, as suggested by the literature [18, 22, 27]; indeed, our numerical simulations corroborate this behavior (Fig. 1.1). Similarly, for the bulk-surface coupled wave-pinning model, Miller et al. employed timescale separation techniques to demonstrate that the interface evolves as an area-preserving geodesic curvature flow [26]. However, for the original wave-pinning model, a rigorous analysis of the slow dynamics is lacking. Consequently, the derivation of a unified interface equation that remains valid across multiple timescales is an open problem.

Through numerical simulations, another intriguing phenomenon regarding the interface motion of the wave-pinning model has been identified: the “shape-sensing phenomenon” [25, 33, 34] (Fig. 1.2). In this process, high-activity domains drift very slowly along the boundary of the domain Ω toward regions of higher curvature. Notably, the timescale of this phenomenon is distinct from, and typically slower than, the curvature flow regime described above. Such geometry-dependent slow motion is not unique to the wave-pinning model; it has been observed in various reaction-diffusion systems, including the Allen-Cahn equation, suggesting it is a universal

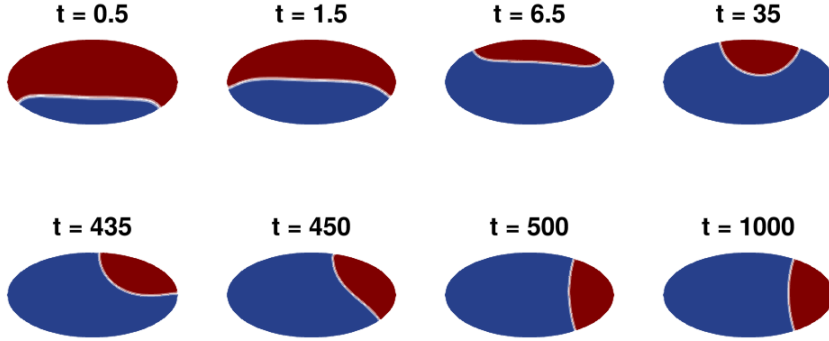


FIG. 1.2. Numerical simulation of (1.1c) on an elliptic domain. The dynamics exhibit a hierarchy of timescales: fast wave propagation, slow area-preserving curvature flow, and very slow drift along the boundary.

behavior driven by the interaction between the interface and the boundary. This type of geometry-dependent slow evolution is classically referred to as “slow dynamics” or “metastability”, which has been extensively studied in the mathematical analysis of reaction-diffusion systems [1, 2, 3, 14, 15]. Biologically, shape-sensing is a well-observed phenomenon; this is summarized in [33]. In parallel, it is suggested to play a pivotal role in the phase-field model of cell motility proposed by [9]. In their model, the migration of the high-activity domain along the cell boundary is essential for driving rotational cell motion. Therefore, providing a theoretical understanding of the internal wave-pinning dynamics—specifically, how the interface interacts with the domain geometry—would offer valuable insights.

Motivated by these considerations, we perform a derivation of more detailed interface equations in \mathbb{R}^2 using the method of matched asymptotic expansions. While Jilkine pioneered the derivation of interface equations incorporating slow timescales [22], we further develop this analysis to explicitly demonstrate the emergence of area-preserving mean curvature flow. More precisely, we derive the following free boundary problem for the interface $\Gamma(t)$, $t > 0$:

$$\begin{aligned}
 (1.2a) \quad & V_n = c(v_0) - \varepsilon[\kappa - \langle \kappa \rangle + \beta(v_0)(v_1 - \langle v_1 \rangle)] & \text{on } \Gamma(t), \quad t \in (0, \infty), \\
 (1.2b) \quad & u_+(v_0)|\Omega_+(t)| + u_-(v_0)|\Omega_-(t)| + v_0|\Omega| = M, & t \in (0, \infty), \\
 (1.2c) \quad & -\Delta v_1 = \frac{(1 + u'_\pm(v_0))\llbracket u_0 \rrbracket}{D\Lambda(v_0)}c(v_0)L & \text{in } \Omega_\pm(t), \quad t \in (0, \infty), \\
 (1.2d) \quad & D\llbracket \partial_n v_1 \rrbracket + c(v_0)\llbracket u_0 \rrbracket = 0 & \text{on } \Gamma(t), \quad t \in (0, \infty), \\
 (1.2e) \quad & \partial_\nu v_1 = 0 & \text{on } \partial\Omega, \quad t \in (0, \infty), \\
 (1.2f) \quad & \int_{\Omega} (u_1 + v_1)dx = 0, \quad u_1 = \frac{\partial_t u_0 - f_v(u_0, v_0)v_1}{f_u(u_0, v_0)}, & t \in (0, \infty).
 \end{aligned}$$

Here, $\Omega_\pm(t)$ denote the subdomains where u is close to the stable states $u_\pm(v_0)$, and we define $u_0 = u_\pm(v_0)$ in $\Omega_\pm(t)$. v_0 and v_1 are the leading- and first-order terms of v . $|\Omega_\pm(t)|$ denotes the area of these subdomains $\Omega_\pm(t)$. The vector n is the unit normal to the interface pointing from $\Omega_+(t)$ to $\Omega_-(t)$. Accordingly, V_n and κ represent the

normal velocity and the mean curvature of the interface, while $\langle \cdot \rangle$ and $[\cdot]$ denote the average and the jump (defined as the value in Ω_+ minus that in Ω_-) across the interface. $c(v_0)$ is the propagating wave speed, M the total mass, D the diffusivity, and L the interface length. Finally, the coefficients $\beta(v_0)$ and $\Lambda(v_0)$ are defined in (2.34) and (2.28), respectively. f_u and f_v denote the partial derivatives of f with respect to u and v , respectively. While we focus on the two-dimensional case, the same argument holds in general N dimensions, with κ replaced by $(N-1)\kappa$. To the best of our knowledge, the derivation of the interface equations that approximate dynamics occurring across multiple timescales has not been established in the literature, with the notable exception of the wave-pinning model. We highlight this as a key mathematical novelty of the present work.

Furthermore, based on the derived free boundary problem, we investigate the behavior of an interface whose endpoints lie on the domain boundary. We demonstrate that such an interface drifts along the boundary toward regions of higher curvature with a speed of $O(\varepsilon^2)$. Specifically, assuming the interface can be approximated by a sufficiently small circular arc, we represent its center using the arc-length parametrization $X^0(s)$ of the boundary $\partial\Omega$. We then show that the evolution of the position $s = s(t)$ is governed by the following approximation:

$$(1.3) \quad \frac{d}{dt} s(t) = \frac{4\varepsilon^2}{3\pi} K_s(s(t)),$$

where K_s denotes the derivative of the curvature K of the boundary $\partial\Omega$ with respect to arc length. In summary, the interface evolves as a propagating front on the $O(1)$ timescale, undergoes area-preserving mean curvature flow on the $O(\varepsilon^{-1})$ timescale, and drifts along the boundary on the $O(\varepsilon^{-2})$ timescale. This hierarchy corresponds to a biological narrative of polarity establishment: First, the cell rapidly establishes a polarized front (fast timescale). Second, the polarized domain relaxes its shape to minimize interfacial tension while preserving its size (slow timescale). Finally, on a much longer timescale, the cell “senses” its geometric confinement, drifting toward regions of high curvature to stabilize its orientation (very slow timescale).

The organization of this paper is as follows. In Section 2 we outline the model assumptions and derive the interface equations (1.2f). In Section 3 we investigate the slow motion of the interface along the domain boundary. We conclude in Section 4 with some final remarks.

2. Formal derivation of the interface equation. In this section we present a formal derivation of the free boundary problem (1.2f) for the wave-pinning model (1.1c). We perform the subsequent analysis under the following three assumptions for the reaction term f , adopting the formulation by [28]:

Bistability condition. For any given v in a certain range $[v_{\min}, v_{\max}]$, the function $f(\cdot, v)$ is bistable. This means that the equation $f(u, v) = 0$ for u has three roots $u_-(v) < u_m(v) < u_+(v)$ for each $v \in [v_{\min}, v_{\max}]$, satisfying

$$(2.1) \quad f_u(u_{\pm}(v), v) < 0, \quad f_u(u_m(v), v) > 0.$$

Homogeneous stability condition. The homogeneous states $(u, v) \equiv (u_{\pm}(v), v)$ for $v \in [v_{\min}, v_{\max}]$ are stable equilibria for the system (1.1c). In their linear stability analysis, Mori, Jilkine, and Edelstein-Keshet [28] observed that this stability condition can be reduced to the following:

$$(2.2) \quad f_u(u_{\pm}(v), v) - f_v(u_{\pm}(v), v) < 0.$$

Velocity sign condition. For the function

$$(2.3) \quad I(v) = \int_{u_-(v)}^{u_+(v)} f(u, v) du,$$

there exists a unique $v_c \in (v_{\min}, v_{\max})$ such that $I(v_c) = 0$, with $I(v)$ being positive for $v > v_c$, negative for $v < v_c$. In addition, it holds that the derivative of I at $v = v_c$ is strictly positive.

The velocity sign condition will be used in Section 3. These conditions are indispensable kinetic requirements for the wave-pinning phenomenon. Another key component for the wave-pinning model is the conservation of the total mass:

$$(2.4) \quad \int_{\Omega} (u + v) dx = M,$$

where

$$M = \int_{\Omega} (u(x, 0) + v(x, 0)) dx.$$

Let $(u^\varepsilon, v^\varepsilon)$ be a solution to (1.1c), and suppose that $v^\varepsilon \in [v_{\min}, v_{\max}]$. On the fast timescale $= \tau = t/\varepsilon$, the leading-order dynamics $\partial_{\tau} u^\varepsilon = f(u^\varepsilon, v^\varepsilon)$ drive u^ε toward the stable states $u_{\pm}(v^\varepsilon)$, leading to the rapid formation of a sharp interface $\Gamma^\varepsilon(t) := \{x \in \Omega \mid u^\varepsilon(x, t) = u_m(v^\varepsilon)\}$ separating the regions $\{u^\varepsilon \approx u_{\pm}(v^\varepsilon)\}$. In what follows, we will derive the equation of motion for the interface $\Gamma^\varepsilon(t)$ that develops on multiple timescales, based on matched asymptotic expansions. Specifically, we employ the additional asymptotic expansion of the signed distance function, as described by Nakamura et al. [29], to derive higher-order approximations for the equation of motion of interfaces. For fundamental concepts and procedures of the method of the matched asymptotic expansions, see, e.g., [7, 13, 29, 32] and references therein.

2.1. Matched asymptotic expansions. We assume that the interface $\Gamma^\varepsilon(t)$ is either a smooth closed curve or a smooth curve whose endpoints lie on the boundary $\partial\Omega$ for every $t \geq 0$. The domain Ω is partitioned into two regions, $\Omega_-^\varepsilon(t) := \{x \in \Omega \mid u^\varepsilon < u_m(v^\varepsilon)\}$ and $\Omega_+^\varepsilon(t) := \{x \in \Omega \mid u^\varepsilon > u_m(v^\varepsilon)\}$. Here, we define the signed distance function to $\Gamma^\varepsilon(t)$ as follows:

$$(2.5) \quad d^\varepsilon(x, t) = \begin{cases} \text{dist}(x, \Gamma^\varepsilon(t)), & x \in \Omega_-^\varepsilon(t), \\ 0, & x \in \Gamma^\varepsilon(t), \\ -\text{dist}(x, \Gamma^\varepsilon(t)), & x \in \Omega_+^\varepsilon(t), \end{cases}$$

where $\text{dist}(x, \Gamma^\varepsilon(t))$ is the distance from $x \in \Omega$ to $\Gamma^\varepsilon(t)$ in \mathbb{R}^2 . Then, we can rewrite

$$\Gamma^\varepsilon(t) = \{x \in \Omega \mid d^\varepsilon(x, t) = 0\}, \quad \Omega_{\pm}^\varepsilon(t) = \{x \in \Omega \mid \pm d^\varepsilon(x, t) < 0\},$$

and define

$$\Gamma^\varepsilon = \bigcup_{t \geq 0} (\Gamma^\varepsilon(t) \times \{t\}), \quad \Omega_{\pm}^\varepsilon = \bigcup_{t \geq 0} (\Omega_{\pm}^\varepsilon(t) \times \{t\}).$$

We assume the following expansions for u and v in the outer region (i.e., away from the interface Γ^ε):

$$(2.6a) \quad u^\varepsilon(x, t) = u_0(x, t) + \varepsilon u_1(x, t) + \varepsilon^2 u_2(x, t) + \dots,$$

$$(2.6b) \quad v^\varepsilon(x, t) = v_0(x, t) + \varepsilon v_1(x, t) + \varepsilon^2 v_2(x, t) + \dots,$$

where the functions u_k and v_k are smooth, bounded and independent of ε for $k = 0, 1, 2, \dots$. These functions satisfy the no-flux boundary condition (1.1c). To be consistent with the total mass M in (2.4), we set

$$(2.7) \quad \int_{\Omega} (u_0 + v_0) dx = M,$$

$$(2.8) \quad \int_{\Omega} (u_k + v_k) dx = 0, \quad k = 1, 2, \dots$$

Let $z(x, t)$ be the stretched variable, defined by $z(x, t) = d^\varepsilon(x, t)/\varepsilon$. Also, let $\gamma(s, t)$ be a parametrization of the interface $\Gamma^\varepsilon(t)$, and $n(s, t)$ be the unit normal vector to $\Gamma^\varepsilon(t)$, pointing from $\Omega_+^\varepsilon(t)$ to $\Omega_-^\varepsilon(t)$. Here, $s \in [0, L]$ is an arc-length parameter along $\Gamma^\varepsilon(t)$, where L is the length of $\Gamma^\varepsilon(t)$. Then, for any point x in the neighborhood of $\Gamma^\varepsilon(t)$, we have the unique expression

$$x = \gamma(s(x, t), t) + \varepsilon z(x, t) n(s(x, t), t).$$

This allows us to introduce the local coordinate system (s, z) near the interface $\Gamma^\varepsilon(t)$. Hence, we assume the following expansions for u and v in the inner region (i.e., near the interface Γ^ε):

$$(2.9a) \quad u^\varepsilon(x, t) = U^\varepsilon(s, z, t) = U_0(s, z, t) + \varepsilon U_1(s, z, t) + \varepsilon^2 U_2(s, z, t) + \dots,$$

$$(2.9b) \quad v^\varepsilon(x, t) = V^\varepsilon(s, z, t) = V_0(s, z, t) + \varepsilon V_1(s, z, t) + \varepsilon^2 V_2(s, z, t) + \dots.$$

where the functions U_k and V_k are smooth and independent of ε for $k = 0, 1, 2, \dots$.

By matching the outer expansions (2.6a), (2.6b) and the inner expansions (2.9a), (2.9b), we require that the following conditions hold for $s \in [0, L]$ and $t > 0$. At the leading order, the large z behavior of the inner solution must match the outer solution at the interface:

$$(2.10a) \quad U_0(s, \pm\infty, t) = u_0(\gamma(s, t) \pm 0, t) + o(1) \quad (z \rightarrow \pm\infty),$$

$$(2.10b) \quad V_0(s, \pm\infty, t) = v_0(\gamma(s, t) \pm 0, t) + o(1) \quad (z \rightarrow \pm\infty).$$

Here, $g(\gamma(s, t) \pm 0)$ denotes the limiting value of an outer function g as $\Gamma^\varepsilon(t)$ is approached from the side where $\pm d(x, t) > 0$, i.e., from $\Omega_+^\varepsilon(t)$. And at the first order, the large z behavior of the inner solution must be linear in z :

$$(2.11a) \quad U_1(s, z, t) = u_1(\gamma(s, t) \pm 0, t) + z \partial_n u_0(\gamma(s, t) \pm 0, t) + o(1) \quad (z \rightarrow \pm\infty),$$

$$(2.11b) \quad V_1(s, z, t) = v_1(\gamma(s, t) \pm 0, t) + z \partial_n v_0(\gamma(s, t) \pm 0, t) + o(1) \quad (z \rightarrow \pm\infty).$$

Furthermore, at the second order, we have

$$(2.12a) \quad \begin{aligned} U_2(s, z, t) &= u_2(\gamma(s, t) \pm 0, t) + z \partial_n u_1(\gamma(s, t) \pm 0, t) \\ &+ \frac{z^2}{2} \partial_n^2 u_0(\gamma(s, t) \pm 0, t) + o(1) \quad (z \rightarrow \pm\infty), \end{aligned}$$

$$(2.12b) \quad \begin{aligned} V_2(s, z, t) &= v_2(\gamma(s, t) \pm 0, t) + z \partial_n v_1(\gamma(s, t) \pm 0, t) \\ &+ \frac{z^2}{2} \partial_n^2 v_0(\gamma(s, t) \pm 0, t) + o(1) \quad (z \rightarrow \pm\infty). \end{aligned}$$

For a derivation of these relations, see the appendix of [7].

We assume the following expansion for d^ε :

$$(2.13) \quad d^\varepsilon(x, t) = d_0(x, t) + \varepsilon d_1(x, t) + \varepsilon^2 d_2(x, t) + \dots,$$

where each function d_k is smooth, bounded and independent of ε for $k = 0, 1, 2, \dots$.

2.2. Leading-order outer and inner solutions.

Outer solutions. Substituting (2.6b) into (1.1c) and collecting the terms of order ε^0 , we obtain

$$(2.14a) \quad f(u_0, v_0) = 0,$$

$$(2.14b) \quad D\Delta v_0 - f(u_0, v_0) = 0.$$

From (2.14a) and bistability of $f(\cdot, v_0)$, it holds that $u_0 = u_{\pm}(v_0)$ or $u_0 = u_m(v_0)$. Now we let

$$(2.15) \quad u_0(x, t) = \begin{cases} u_-(v_0), & x \in \Omega_-^\varepsilon(t), \\ u_+(v_0), & x \in \Omega_+^\varepsilon(t), \end{cases}$$

at time $t > 0$. Adding (2.14a) and (2.14b) yields $D\Delta v_0 = 0$ in $\Omega_-^\varepsilon(t)$ and $\Omega_+^\varepsilon(t)$, which, together with (1.1c), implies that v_0 is spatially uniform in $\Omega_-^\varepsilon(t)$ and $\Omega_+^\varepsilon(t)$. We denote

$$(2.16) \quad v_0(x, t) = \begin{cases} v_<(t), & x \in \Omega_-^\varepsilon(t), \\ v_>(t), & x \in \Omega_+^\varepsilon(t). \end{cases}$$

Inner solutions. Note that $|\nabla d^\varepsilon| = 1$, $\nabla s \cdot \nabla d^\varepsilon = 0$, $|\nabla s|^2 = 1 + O(\varepsilon)$, $\Delta s = O(\varepsilon)$, and $\Delta d^\varepsilon = \kappa - \varepsilon \kappa^2 z + O(\varepsilon^2)$, where $\kappa = \kappa(s, t)$ is the curvature of $\Gamma^\varepsilon(t)$. Using these relations and the chain rule, we obtain the following relations for (2.9a) (and likewise for (2.9b)) hold:

$$\begin{aligned} \partial_t u^\varepsilon &= \frac{1}{\varepsilon} \partial_t d^\varepsilon \partial_z U^\varepsilon + \partial_t s \partial_s U^\varepsilon + \partial_t U^\varepsilon, \\ \Delta u^\varepsilon &= \frac{1}{\varepsilon^2} \partial_z^2 U^\varepsilon + \frac{1}{\varepsilon} \kappa \partial_z U^\varepsilon + \partial_s^2 U^\varepsilon - \kappa^2 z \partial_z U^\varepsilon + O(\varepsilon). \end{aligned}$$

Thus, substituting (2.9b) into (1.1b) and collecting the terms of order ε^{-2} , we therefore obtain

$$(2.17) \quad D\partial_z^2 V_0 = 0,$$

From (2.17), V_0 is represented as

$$V_0 = a(t)z + b(t),$$

where a and b are real functions of time t . However, the matching condition (2.10b) implies that V_0 remains bounded as $z \rightarrow \pm\infty$, leading to $a(t) = 0$ and $b(t) = v_<(t) = v_>(t)$. Therefore, V_0 reduces to the spatially uniform function v_0 :

$$(2.18) \quad V_0(t) = v_0(t).$$

We derive the governing equation for v_0 . Integrating $u_0 + v_0$ over Ω with (2.15) yields:

$$\int_{\Omega} (u_0 + v_0) dx = u_+(v_0) |\Omega_+^\varepsilon(t)| + u_-(v_0) |\Omega_-^\varepsilon(t)| + v_0 |\Omega|,$$

where $|\Omega|$ represents the area of Ω and similarly for the subdomains. Thus, the mass conservation law (2.7) reduces to

$$(2.19) \quad u_+(v_0) |\Omega_+^\varepsilon(t)| + u_-(v_0) |\Omega_-^\varepsilon(t)| + v_0 |\Omega| = M,$$

which determines v_0 .

Next, we consider the inner solutions for u . Substituting (2.9a) into (1.1a) and collecting the terms of order ε^0 , we obtain

$$(2.20) \quad \partial_z^2 U_0 - \partial_t d_0 \partial_z U_0 + f(U_0, V_0) = 0.$$

From the matching condition (2.10a), U_0 is characterized as a heteroclinic solution from $u_+(V_0)$ toward $u_-(V_0)$. Multiplying (2.20) by $\partial_z U_0$ and integrating over $z \in \mathbb{R}$, we obtain

$$(2.21) \quad -\partial_t d_0 = c(V_0) := \frac{\int_{u_-(V_0)}^{u_+(V_0)} f(u, V_0) du}{\int_{\mathbb{R}} (\partial_z U_0)^2 dz}.$$

Note that U_0 depends only on z and V_0 . Therefore, we write $U_0 = U_0(z, V_0)$.

2.3. First-order outer and inner solutions.

Outer solutions. Substituting (2.6a) into (1.1a) and collecting the terms of order ε^1 , we obtain

$$(2.22a) \quad \partial_t u_0 = f_u(u_0, v_0)u_1 + f_v(u_0, v_0)v_1,$$

$$(2.22b) \quad \partial_t v_0 = D\Delta v_1 - f_u(u_0, v_0)u_1 - f_v(u_0, v_0)v_1.$$

Adding (2.22a) and (2.22b), we obtain

$$(2.23) \quad D\Delta v_1 = \partial_t(u_0 + v_0).$$

We now derive the solvability condition for the Poisson equation (2.23) by integrating it over the entire domain Ω . First, we evaluate the left-hand side. Applying the divergence theorem and using the no-flux boundary condition for v_1 on $\partial\Omega$, the integral of the Laplacian term is reduced to an integral over the interface $\Gamma^\varepsilon(t)$:

$$(2.24) \quad \int_{\Omega} \Delta v_1 dx = \int_{\Gamma^\varepsilon(t)} [\partial_n v_1] ds.$$

Here, $[\![g]\!]$ denotes the jump of a quantity $g = g(x, t)$ across the interface $\Gamma^\varepsilon(t)$, defined as $[\![g]\!] := g(\gamma(s, t) - 0, t) - g(\gamma(s, t) + 0, t)$ for $s \in [0, L]$ and $t > 0$.

Next, we evaluate the right-hand side. The total mass of the leading order terms is conserved as in (2.7). Applying the Reynolds transport theorem relates this conservation law to the source term:

$$0 = \frac{d}{dt} \int_{\Omega} (u_0 + v_0) dx = \int_{\Omega} \partial_t(u_0 + v_0) dx + [\![u_0]\!] \int_{\Gamma^\varepsilon(t)} V_n ds,$$

where $V_n = V_n(s, t)$ is the normal velocity of the interface $\Gamma^\varepsilon(t)$. From this equation, we have

$$(2.25) \quad \int_{\Omega} \partial_t(u_0 + v_0) dx = -[\![u_0]\!] \int_{\Gamma^\varepsilon(t)} V_n ds.$$

Therefore, as a solvability condition for (2.23), we conclude that

$$(2.26) \quad \int_{\Gamma^\varepsilon(t)} (D[\![\partial_n v_1]\!] + [\![u_0]\!] V_n) ds = 0.$$

We also need to rewrite the right-hand side of the Poisson equation (2.23) with another form, which is $\partial_t(u_0 + v_0)$ now. We rewrite (2.25) as

$$(2.27) \quad \Lambda(v_0)\partial_t v_0 = -\llbracket u_0 \rrbracket \dot{A},$$

where $\dot{A} := \int_{\Gamma^\varepsilon(t)} V_n ds$ is the time derivative of the area of the subdomain $\Omega_+^\varepsilon(t)$,

$$(2.28) \quad \Lambda(v_0) := u'_+(v_0)|\Omega_+^\varepsilon(t)| + u'_-(v_0)|\Omega_-^\varepsilon(t)| + |\Omega|$$

and the prime ('') denotes the derivative with respect to v_0 .

We claim that $\Lambda(v_0)$ is positive. To show this, we differentiate $f(u_\pm(v), v) = 0$ with respect to v to obtain $f_u(u_\pm(v), v)u'_\pm(v) + f_v(u_\pm(v), v) = 0$. The stability condition (2.2) ensures that $f_v(u_\pm(v), v) > f_u(u_\pm(v), v)$, which leads to the inequality

$$(1 + u'_\pm(v))f_u(u_\pm(v), v) < 0.$$

For this product to be negative under (2.1), we must conclude that $1 + u'_\pm(v) > 0$, which confirms the positivity of $\Lambda(v_0)$. Combined with (2.27), this implies that $\partial_t v_0$ and \dot{A} have opposite signs, that is, v_0 decreases as the subdomain $\Omega_+^\varepsilon(t)$ expands.

We also calculate $\partial_t u_0 = u'_\pm(v_0)\partial_t v_0$ in Ω_\pm^ε . Thus, $\partial_t(u_0 + v_0) = (1 + u'_\pm(v_0))\partial_t v_0$ holds and the Poisson equation (2.23) can be rewritten into

$$(2.29) \quad -\Delta v_1 = \frac{(1 + u'_\pm(v_0))\llbracket u_0 \rrbracket}{D\Lambda(v_0)} \dot{A} \quad \text{in } \Omega_\pm^\varepsilon$$

by using (2.27).

Inner solutions. Substituting (2.9b) into (1.1b) and collecting the terms of order ε^{-1} , we obtain

$$(2.30) \quad D(\partial_z^2 V_1 + \kappa \partial_z V_0) = 0.$$

Since $\partial_z V_0 = 0$, we obtain $D\partial_z^2 V_1 = 0$. By an argument analogous to the one for V_0 , we conclude that v_1 is continuous on the interface $\Gamma^\varepsilon(t)$ and V_1 is constant in z :

$$(2.31) \quad V_1(s, z, t) = v_1(\gamma(s, t), t), \quad s \in [0, L], t > 0.$$

Substituting (2.9a) into (1.1a) and collecting the terms of order ε^1 , we obtain

$$(2.32) \quad \begin{aligned} & \partial_z^2 U_1 - \partial_t d_0 \partial_z U_1 + f_u(U_0, V_0) U_1 \\ &= \partial_t s \partial_s U_0 + \partial_t U_0 + \partial_t d_1 \partial_z U_0 - \kappa \partial_z U_0 - f_v(U_0, V_0) V_1. \end{aligned}$$

Let \mathcal{L} be an operator on $L^2(\mathbb{R})$ defined by $\mathcal{L} := \partial_z^2 - (\partial_t d_0)\partial_z + f_u(U_0, V_0)$, and $h \in L^2(\mathbb{R})$ be the right-hand side of (2.32). Then, we can rewrite (2.32) as $\mathcal{L}U_1 = h$, i.e., h is in the range of \mathcal{L} . Differentiating (2.20) with respect to z , we also see that $\mathcal{L}(\partial_z U_0) = 0$. Thus, for the adjoint operator of \mathcal{L} denoted by $\mathcal{L}^* = \partial_z^2 + (\partial_t d_0)\partial_z + f_u(U_0, V_0)$, $p^*(z) = \partial_z U_0(-z)$ satisfies $\mathcal{L}^* p^* = 0$, i.e., p^* is in the kernel of \mathcal{L}^* . Since the range of \mathcal{L} is orthogonal to the kernel of its adjoint \mathcal{L}^* , we have

$$\int_{\mathbb{R}} (\partial_t U_0 + (\partial_t d_1 - \kappa) \partial_z U_0 - f_v(U_0, V_0) V_1) p^* dz = 0,$$

where we used the fact that $\partial_s U_0 = 0$. Therefore, we conclude that

$$(2.33) \quad \begin{aligned} -\partial_t d_1 &= -\kappa + \frac{\int_{\mathbb{R}} (\partial_t U_0 - f_v(U_0, V_0) V_1) \partial_z U_0(-z) dz}{\int_{\mathbb{R}} \partial_z U_0(z) \partial_z U_0(-z) dz} \\ &= -\kappa + \alpha(V_0) - \beta(V_0) V_1, \end{aligned}$$

where

$$(2.34) \quad \alpha(V_0) = \frac{\int_{\mathbb{R}} \partial_t U_0 \partial_z U_0(-z) dz}{\int_{\mathbb{R}} \partial_z U_0(z) \partial_z U_0(-z) dz}, \quad \beta(V_0) = \frac{\int_{\mathbb{R}} f_v(U_0, V_0) \partial_z U_0(-z) dz}{\int_{\mathbb{R}} \partial_z U_0(z) \partial_z U_0(-z) dz}.$$

2.4. The interface equation. Using the relation $V_n = -\partial_t d^\varepsilon = -\partial_t d_0 - \varepsilon \partial_t d_1 + O(\varepsilon^2)$, (2.21) and (2.33) yield the following approximate interface equation for Γ^ε :

$$(2.35) \quad V_n = c(v_0) - \varepsilon (\kappa - \alpha(v_0) + \beta(v_0)v_1) \quad \text{on } \Gamma^\varepsilon.$$

We note that the Poisson equation (2.29) for v_1 has a unique solution subject to the no-flux boundary condition (1.1c), the mass conservation law (2.8), and continuity across the interface $\Gamma^\varepsilon(t)$. Here, the term u_1 appearing in the conservation law (2.8) is explicitly obtained from (2.22a).

If the interface touches the boundary $\partial\Omega$ at its endpoints, the no-flux boundary condition (1.1c) ensures that the interface meets the boundary $\partial\Omega$ orthogonally [32].

Lastly, we shall simplify the interface equation (2.35). To this end, we begin by deriving the pointwise jump relation between u_0 and $\partial_n v_1$ from the matching of outer and inner solutions. Integrating (2.20) over \mathbb{R} and using (2.10a), we obtain

$$(2.36) \quad \int_{\mathbb{R}} f(U_0, v_0) dz = c(v_0) \llbracket u_0 \rrbracket.$$

Next, substituting (2.9b) into (1.1b) and collecting the term of order ε^0 , we obtain

$$(2.37) \quad f(U_0, v_0) = D \partial_z^2 V_2.$$

Integrating this equation over \mathbb{R} and using the second-order matching condition (2.12b), we obtain

$$(2.38) \quad \int_{\mathbb{R}} f(U_0, v_0) dz = -D \llbracket \partial_n v_1 \rrbracket.$$

Therefore, (2.36) and (2.38) lead to the following relation:

$$(2.39) \quad D \llbracket \partial_n v_1 \rrbracket + c(v_0) \llbracket u_0 \rrbracket = 0.$$

We now compare this jump relation with the solvability condition (2.26) for v_1 , discarding terms of order $O(\varepsilon^2)$ of V_n , yielding

$$(2.40) \quad \llbracket u_0 \rrbracket \int_{\Gamma^\varepsilon(t)} (-\kappa + \alpha(v_0) - \beta(v_0)v_1) ds = 0.$$

Since $\alpha(v_0)$ and $\beta(v_0)$ are spatially constants, (2.40) gives the expression for $\alpha(v_0)$:

$$(2.41) \quad \alpha(v_0) = \langle \kappa \rangle + \beta(v_0) \langle v_1 \rangle,$$

where $\langle \kappa \rangle$ is the average of κ over the interface $\Gamma^\varepsilon(t)$ and likewise for $\langle v_1 \rangle$. Consequently, we arrive at the final form of the interface equation:

$$(2.42) \quad V_n = c(v_0) - \varepsilon [\kappa - \langle \kappa \rangle + \beta(v_0)(v_1 - \langle v_1 \rangle)].$$

Equation (2.42) encapsulates the interplay of forces acting on the interface. The term proportional to κ represents the surface tension effect that drives the curvature flow,

minimizing the interface length. The non-local average term $\langle \kappa \rangle$ acts as a global Lagrange multiplier that enforces the area preservation, counteracting the shrinking effect of the curvature flow. The deviation term involving v_1 represents higher-order mass transport effects. By virtue of this consequence of the area preservation on the slow timescale, we obtain that $\dot{A} = c(v_0)L$, allowing us to rewrite (2.23) as (1.2c).

This resulting equation reveals that the interface dynamics involve two distinct timescale effects: a dominant $O(1)$ motion propagating at speed $c(v_0)$, and a slower $O(\varepsilon)$ modulation driven by area-preserving curvature flow and higher-order terms.

We summarize our analysis in the following.

THEOREM 2.1. *Assume the reaction term f satisfies (2.1) and (2.2). Let $(u^\varepsilon, v^\varepsilon)$ be a solution to the wave-pinning model (1.1c) consistent with the matched asymptotic expansions defined in (2.6b) and (2.9b). Then, the dynamics of the interface Γ^ε of the solution u^ε is approximated by the free boundary problem (1.2f) up to $O(\varepsilon^2)$.*

3. Slow interface motion along the boundary. In this section, we show that the interface, which intersects the boundary orthogonally and evolves according to (2.42), moves toward a local maximum of the boundary curvature. Our analysis employs a perturbation method for an interface enclosing a small area, following the approach of Alikakos et al. [1]

Let $\Omega \subset \mathbb{R}^2$ be a bounded domain with smooth boundary $\partial\Omega$ of class C^4 . We consider a family of smooth simple curves $\{\Gamma(t)\}_{t \geq 0}$, which evolve according to the interface equation (2.42). Each curve $\Gamma(t)$ intersects the boundary $\partial\Omega$ orthogonally at its endpoints, and separates the domain into $\Omega_+(t)$ and $\Omega_-(t)$. We assume that the evolution of the interface is in a quasi-static regime. More precisely, we consider the case where the interface evolves slowly with a speed of $O(\varepsilon)$, or equivalently, the magnitude of the leading-order velocity $c(v_0)$ is $O(\varepsilon)$. In such a slow regime, the interface tends to remain close to a stable equilibrium state. Indeed, numerical simulations (Fig. 1.2) suggest that the interface evolves while maintaining a shape sufficiently close to a circular arc. Based on this observation, we assume that $\Gamma(t)$ is close to a circular arc. To localize our analysis, we also assume that the size of the nearly circular interface is sufficiently small; specifically, we consider the case where the interface length L is of order ε . Under these assumptions, the free boundary problem (1.2f) reduces to the following simplified form, independent of v_1 .

$$(3.1a) \quad V_n = c(v_0) - \varepsilon(\kappa - \langle \kappa \rangle) + O(\varepsilon^3) \quad \text{on } \Gamma(t), t > 0,$$

$$(3.1b) \quad u_+(v_0)|\Omega_+(t)| + u_-(v_0)|\Omega_-(t)| + v_0|\Omega| = M \quad t \geq 0.$$

Here, v_1 is assumed to be small and is absorbed into the $O(\varepsilon^3)$ term. While a rigorous derivation of the L^∞ bounds for v_1 requires a detailed analysis of the transmission problem with jump condition (2.39), the scaling behavior can be understood as follows. Recall that v_1 satisfies the Poisson equation (2.29), where the source term is proportional to $c(v_0)L$. Given the assumptions that $c(v_0)$ and L are of order ε , the product $c(v_0)L$ scales as $O(\varepsilon^2)$. Thus, standard elliptic regularity estimates suggest that the magnitude of v_1 is controlled by this source term, justifying the ansatz $v_1 = O(\varepsilon^2)$. For simplicity, we rename T back to t and hereafter identify \mathbb{R}^2 with \mathbb{C} .

In what follows, we introduce a conformal mapping that flattens the curved boundary, thereby transferring our analysis to the complex upper half-plane. In this setting, we treat the interface as a perturbation of a semi-circle and compute the relevant geometric quantities, such as the normal velocity and mean curvature. Finally, applying these to the reduced free boundary problem, we demonstrate that the in-

terface moves along the boundary driven by the gradient of the boundary curvature, and we establish the stability of the near-circular configuration.

3.1. Conformal mapping. Analyzing interface motion near a general curved boundary is analytically challenging due to the complexity of the Neumann boundary condition. To overcome this, we employ a conformal mapping technique. This allows us to “flatten” the boundary geometry, transforming the complex domain interactions into a tractable perturbation problem on the upper half-plane.

Let $X^0(s)$, $s \in \mathbb{R}/L\mathbb{Z}$, be an arc-length parametrization of $\partial\Omega$, where L is the length of $\partial\Omega$. Since the boundary $\partial\Omega$ is of class C^4 , X^0 is also in $C^4(\mathbb{R}/L\mathbb{Z})$. Let $z_0 \in \Omega$ be an arbitrary point. We denote the upper half-plane of \mathbb{C} as \mathbb{H} . Then, there exists a unique conformal diffeomorphism $\Psi: \mathbb{H} \times \mathbb{R}/L\mathbb{Z} \rightarrow \overline{\Omega}$ satisfying the following properties for every $s \in \mathbb{R}/L\mathbb{Z}$:

- $\Psi(\cdot, s)$ maps the real line onto $\partial\Omega$ and a point on the positive imaginary axis to the point z_0 .
- $\Psi(0, s) = X^0(s)$, $\Psi_\zeta(0, s) = \tau(s) := X_s^0(s)$.

This conformal mapping is also of class C^4 , and its existence and uniqueness are guaranteed by the Riemann mapping theorem. The overall approach for this mapping, including the derivation of its properties, is detailed in Alikakos et al. [1].

For any fixed $s_0 \in \mathbb{R}/L\mathbb{Z}$, let $g(s, s_0)$ be the real-valued smooth function satisfying

$$(3.2) \quad X^0(s + s_0) = \Psi(g(s, s_0), s_0), \quad s \in (-L/4, L/4).$$

From the definition of Ψ , we have $g(0, s_0) = 0$. The Taylor expansion of $\Psi(g(s, s_0), s_0)$ around $s = 0$ yields

$$(3.3) \quad \begin{aligned} \Psi(g(s, s_0), s_0) = & X^0(s_0) + \Psi_\zeta g_s s + \frac{1}{2} (\Psi_{\zeta\zeta} g_s^2 + \Psi_\zeta g_{ss}) s^2 \\ & + \frac{1}{6} (\Psi_{\zeta\zeta\zeta} g_s^3 + 3\Psi_{\zeta\zeta} g_{ss} g_s + \Psi_\zeta g_{sss}) s^3 + O(s^4), \end{aligned}$$

where all the derivatives are evaluated at $\zeta = 0$ and at $s = 0$. The Taylor expansion of $X^0(s + s_0)$ around $s = 0$ also yields

$$(3.4) \quad X^0(s + s_0) = X^0(s_0) + \tau s + \frac{1}{2} iK\tau s^2 + \frac{1}{6} (iK_s - K^2) \tau s^3 + O(s^4),$$

where we have used the relations $X_s^0 = \tau$, $X_{ss}^0 = \tau_s = -K\nu = iK\tau$, and $X_{sss}^0 = i(K\tau)_s = i(K_s\tau + iK^2\tau)$. Here, K is the curvature and ν is the unit outward normal vector of the boundary $\partial\Omega$. i is the imaginary unit. All terms on the right-hand side of (3.4) are evaluated at $s = 0$.

Comparing the coefficients of the expansions (3.3) and (3.4) according to (3.2), we deduce that $g_s(0, s_0) = 1$, and

$$\begin{aligned} \Psi_{\zeta\zeta}(0, s_0) &= (iK(s_0) - g_{ss}(0, s_0)) \tau(s_0) =: a(s_0) \tau(s_0), \\ \Psi_{\zeta\zeta\zeta}(0, s_0) &= (i(K_s(s_0) - 3K(s_0)g_{ss}(0, s_0)) + 3g_{ss}^2(0, s_0) - g_{sss}(0, s_0) - K^2(s_0)) \tau(s_0) \\ &=: b(s_0) \tau(s_0). \end{aligned}$$

Since Ψ is of class C^4 up to the real axis, for sufficiently small ζ , we conclude that

$$\Psi(\zeta, s) = X^0(s) + \tau(s) \left(\zeta + \frac{1}{2} a(s) \zeta^2 + \frac{1}{6} b(s) \zeta^3 + O(\zeta^4) \right).$$

Writing $a(s) = a_1(s) + ia_2(s)$ and $b(s) = b_1(s) + ib_2(s)$, where a_k and b_k are real-valued function for $k = 1, 2$, we see that

$$\begin{aligned} a_1(s) &= -g_{ss}(0, s), & a_2(s) &= K(s), \\ b_1(s) &= 3g_{ss}^2(0, s) - g_{sss}(0, s) - K^2(s), & b_2(s) &= K_s(s) - 3K(s)g_{ss}(0, s). \end{aligned}$$

3.2. Representation of the interface. As mentioned at the beginning of this section, we consider the situation in which the interface $\Gamma(t)$ is sufficiently close to a circular arc with a perimeter of order ε , which is small enough to allow the boundary $\partial\Omega$ to be locally approximated as flat on the scale of $\Gamma(t)$. Specifically, we parametrize the interface $\Gamma(t)$ as follows:

$$(3.5) \quad \Gamma(t) = \{\Psi(\zeta, s) \mid \zeta = \varepsilon e^{\varepsilon^2 R(\theta, t) + i\theta}, s = s(t), 0 \leq \theta \leq \pi\},$$

where the unknown $R = R(\theta, t)$ is a smooth function representing the perturbation, and the unknown $s(t)$ is smooth and describes the center of the semicircle. This parametrization effectively reduces the dynamics of $\Gamma(t)$ along the boundary to the dynamics of $s(t)$.

Since the interface touches the boundary orthogonally, we expand the perturbation $R(\theta, t)$ as a Fourier cosine series:

$$(3.6) \quad R(\theta, t) = R_0(t) + \sum_{n \geq 2} R_n(t) \cos(n\theta).$$

The $n = 1$ mode, which corresponds to a shift of the center, is omitted from this expansion since it is handled by $s(t)$.

3.3. Propagating wave speed $c(v_0)$. Based on the parametrization for $\Gamma(t)$ as in (3.5), we write v_0 and $c(v_0)$ in terms of R_0 . As a first step, we calculate the area of the droplet enclosed by $\Gamma(t)$ and a segment of $\partial\Omega$. We now let $\Omega_+(t)$ correspond to the droplet. One can also choose $\Omega_-(t)$ as the droplet; the choice is of no consequence to the following analysis except for the signs of geometric quantities. Let D_+ be the domain in the mapped coordinates, $D_+ := \{re^{i\theta} \mid 0 \leq r \leq \varepsilon e^{\varepsilon^2 R(\theta, t)}, 0 \leq \theta \leq \pi\}$. The area is then:

$$\begin{aligned} |\Omega_+(t)| &= |\Psi(D_+, s)| = \int_{\Psi(D_+, s)} dw = \int_{D_+} |\Psi_\zeta|^2 d\zeta \\ &= \int_{D_+} |1 + a\zeta + b\zeta^2/2 + O(\zeta^3)|^2 d\zeta \\ &= \int_0^\pi \int_0^{\varepsilon e^{\varepsilon^2 R}} |1 + are^{i\theta} + br^2 e^{2i\theta}/2 + O(r^3)|^2 r dr d\theta \\ &= \frac{\pi}{2} \varepsilon^2 - \frac{4}{3} \varepsilon^3 K + \pi \varepsilon^4 \left[R_0 + \frac{1}{4} (a_1^2 + a_2^2) \right] + O(\varepsilon^5). \end{aligned}$$

Therefore, the area can be considered a function in terms of R_0 .

Next, we denote the left-hand side of (3.1b) by $F(v_0, R_0)$. The partial derivative of F with respect to v_0 is given by $\Lambda(v_0)$ in (2.28). Since $\Lambda(v_0)$ is positive, the Implicit Function Theorem guarantees the existence of a unique function $v_0 = v_0(R_0)$ satisfying $F(v_0(R_0), R_0) = M$. In addition, we have

$$\begin{aligned} F_{R_0} &= u_+(v_0) \partial_{R_0} |\Omega_+(t)| + u_-(v_0) \partial_{R_0} (|\Omega| - |\Omega_+(t)|) \\ &= (u_+(v_0) - u_-(v_0))(\pi \varepsilon^4 + O(\varepsilon^5)) > 0, \end{aligned}$$

leading to

$$(3.7) \quad v'_0(R_0) = -\frac{F_{R_0}}{F_{v_0}} < 0.$$

Here, the prime (') also denotes the derivative with respect to R_0 .

To be consistent with the assumption that $c(v_0)$ is of order ε , we introduce a function $w_\varepsilon(R_0)$ of order ε^0 such that

$$(3.8) \quad v_0(R_0) = v_c + \varepsilon w_\varepsilon(R_0),$$

where v_c is a constant satisfying $c(v_c) = 0$ and $c'(v_c) > 0$ (see the velocity sign condition). Accordingly, We expand $c(v_0)$ into a Taylor series to obtain:

$$(3.9) \quad c(v_0) = \varepsilon c'(v_c) w_\varepsilon(R_0) + O(\varepsilon^2 w_\varepsilon^2).$$

It is clear that $w_\varepsilon(R_0)$ also satisfies $w'_\varepsilon(R_0) < 0$.

3.4. Geometric quantities. We now calculate the normal velocity V_n and curvature κ of the interface $\Gamma(t)$, which is parametrized by (3.5). We denote a point on the interface by $x(\theta, t) + iy(\theta, t) = z(\theta, t) = \Psi(\zeta, s(t))$, where $\zeta = \varepsilon e^{\varepsilon^2 R(\theta, t) + i\theta}$. The unit normal vector is taken to point from the droplet region $\Omega_+(t)$ to $\Omega_-(t)$.

First, we calculate the normal velocity V_n . The normal velocity is given by

$$\begin{aligned} V_n(\theta, t) &= \frac{x_t y_\theta - x_\theta y_t}{|z_\theta|} = -\frac{\operatorname{Im}(z_t \bar{z}_\theta)}{|z_\theta|} \\ &= -\frac{\operatorname{Im}((\Psi_\zeta \zeta_t + \Psi_s \dot{s}) \bar{\Psi}_\zeta \bar{\zeta}_\theta)}{|\Psi_\zeta \zeta_\theta|} = -\frac{\operatorname{Im}((|\Psi_\zeta|^2 \zeta_t + \Psi_s \bar{\Psi}_\zeta \dot{s}) \bar{\zeta}_\theta)}{|\Psi_\zeta \zeta_\theta|}. \end{aligned}$$

Here, the dot (.) denotes the derivative with respect to time t . We see that

$$\begin{aligned} \Psi_\zeta &= \tau + O(\zeta), & \Psi_s &= \tau + O(\zeta), \\ \zeta_\theta &= (\varepsilon^2 R_\theta + i)\zeta, & \dot{\zeta} &= \varepsilon^2 \dot{R} \zeta. \end{aligned}$$

Substituting these into the formula for V_n yields

$$(3.10) \quad V_n(\theta, t) = \dot{s} (\cos \theta + \varepsilon B_1^\varepsilon) + \varepsilon^3 \dot{R} (1 + \varepsilon B_2^\varepsilon)$$

where B_i^ε is a function of order ε^0 for $i = 1, 2$.

Next, we calculate the curvature κ of $\Gamma(t)$. The curvature is given by

$$\kappa(\theta, t) = \frac{y_{\theta\theta} x_\theta - x_{\theta\theta} y_\theta}{|z_\theta|^3} = \frac{\operatorname{Im}(z_{\theta\theta} \bar{z}_\theta)}{|z_\theta|^3} = \frac{\operatorname{Im}(\zeta_{\theta\theta} \bar{\zeta}_\theta)}{|\Psi_\zeta||\dot{\zeta}_\theta|^3} + \frac{\operatorname{Im}(\Psi_\zeta \bar{\Psi}_\zeta \zeta_\theta)}{|\Psi_\zeta|^3 |\zeta_\theta|}.$$

Taking $\zeta = O(\varepsilon)$ into account, each component can be calculated as follows:

$$\begin{aligned} |\Psi_\zeta|^2 &= |1 + a\zeta + b\zeta^2/2 + O(\zeta^3)|^2 \\ &= 1 + 2\operatorname{Re}(a\zeta + b\zeta^2/2) + |a\zeta|^2 + O(\varepsilon^3), \end{aligned}$$

$$|\zeta_\theta| = \sqrt{1 + \varepsilon^4 R_\theta^2} |\zeta|,$$

$$\begin{aligned} \operatorname{Im}(\zeta_{\theta\theta} \bar{\zeta}_\theta) &= \operatorname{Im}((\varepsilon^4 R_\theta^2 + \varepsilon^2 R_{\theta\theta} - 1 + 2i\varepsilon^2 R_\theta)(\varepsilon^2 R_\theta - i)) |\zeta|^2 \\ &= (1 - \varepsilon^2 R_{\theta\theta} + O(\varepsilon^4)) |\zeta|^2, \end{aligned}$$

$$\begin{aligned} \operatorname{Im}(\Psi_\zeta \bar{\Psi}_\zeta \zeta_\theta) &= \operatorname{Im}((a + b\zeta + O(\zeta^2)) \overline{(1 + a\zeta + b\zeta^2/2 + O(\zeta^3))} (\varepsilon^2 R_\theta + i)\zeta) \\ &= \operatorname{Re}(a\zeta) + |a\zeta|^2 + \operatorname{Re}(b\zeta^2) + O(\varepsilon^3). \end{aligned}$$

We then obtain that

$$\frac{\text{Im}(\zeta_{\theta\theta}\bar{\zeta}_\theta)}{|\zeta_\theta|^3|\Psi_\zeta|} = \frac{1}{\varepsilon} \left[1 - \text{Re}(a\zeta) - \varepsilon^2 R_{\theta\theta} - \frac{1}{2} (\text{Re}(b\zeta^2) + |a\zeta|^2 - 3\text{Re}(a\zeta)^2) - \varepsilon^2 R + O(\varepsilon^3) \right],$$

$$\frac{\text{Im}(\Psi_{\zeta\zeta}\bar{\Psi}_{\zeta\zeta}\zeta_\theta)}{|\zeta_\theta||\Psi_\zeta|^3} = \frac{1}{\varepsilon} [\text{Re}(a\zeta) + |a\zeta|^2 + \text{Re}(b\zeta^2) - 3\text{Re}(a\zeta)^2 + O(\varepsilon^3)].$$

Therefore, we have

$$\begin{aligned} \kappa &= \frac{1}{\varepsilon} \left[1 - \varepsilon^2 (R_{\theta\theta} + R) + \frac{1}{2} (|a\zeta|^2 + \text{Re}(b\zeta^2) - 3\text{Re}(a\zeta)^2) + O(\varepsilon^3) \right] \\ &= \frac{1}{\varepsilon} \left[1 - \varepsilon^2 (R_{\theta\theta} + R) + \frac{\varepsilon^2}{2} (|a|^2 + \text{Re}(be^{2i\theta}) - 3\text{Re}(ae^{i\theta})^2) + O(\varepsilon^3) \right]. \end{aligned}$$

Now we use the facts

$$\sin(2\theta) = \sum_{k=0}^{\infty} \frac{8}{\pi(3-4k-4k^2)} \cos((2k+1)\theta), \quad b_2 - 3a_1a_2 = K_s,$$

then we obtain that

$$(3.11) \quad \kappa = \frac{1}{\varepsilon} - \varepsilon \left(R_0 + \sum_{n \geq 2} (1 - n^2) R_n \cos(n\theta) \right) - \frac{\varepsilon}{2} \sum_{n \geq 0} e_n(s) \cos(n\theta) + O(\varepsilon^2),$$

where

$$e_n(s) = \begin{cases} \frac{1}{2}(a_1^2(s) + a_2^2(s)), & n = 0, \\ -b_1(s) + \frac{3}{2}(a_1^2(s) - a_2^2(s)), & n = 2, \\ \frac{8K_s(s)}{\pi(3-4k-4k^2)}, & n = 2k+1, k \geq 0, \\ 0 & n = 2k, k \geq 2. \end{cases}$$

This expression implies that

$$(3.12) \quad \langle \kappa \rangle = \frac{1}{\varepsilon} - \varepsilon R_0 - \frac{\varepsilon}{4} (a_1^2 + a_2^2) + O(\varepsilon^2),$$

that is, $\langle \kappa \rangle$ extracts 0-mode from κ .

3.5. Motion along the boundary. Substituting (3.9)–(3.12) into (3.1a), we obtain

$$\begin{aligned} &\dot{s}(\cos\theta + \varepsilon B_1^\varepsilon) + \varepsilon^3 \dot{R}(1 + \varepsilon B_2^\varepsilon) \\ &= \varepsilon c'(v_c) w_\varepsilon(R_0) + \varepsilon^2 C_1^\varepsilon + \varepsilon^2 \sum_{n \geq 2} (1 - n^2) R_n \cos(n\theta) + \frac{\varepsilon^2}{2} \sum_{n \geq 1} e_n \cos(n\theta) + \varepsilon^3 B_3^\varepsilon, \end{aligned}$$

where C_1^ε represents the 0-mode terms of order w_ε^2 , and B_3^ε collects the terms without the 0-mode. Dividing both sides by $1 + \varepsilon B_2^\varepsilon$ yields

$$\begin{aligned} (3.13) \quad &\varepsilon \left(\varepsilon^2 \dot{R}_0 - c'(v_c) w_\varepsilon(R_0) \right) + \left(\dot{s} - \frac{4\varepsilon^2}{3\pi} K_s \right) \cos\theta + \varepsilon^2 \sum_{n \geq 2} E_n(s, t) \cos(n\theta) \\ &= \varepsilon^2 C_2^\varepsilon + \varepsilon B_5^\varepsilon \dot{s} + \varepsilon^3 B_6^\varepsilon, \end{aligned}$$

where C_2^ε denotes the 0-mode terms of order w_ε^2 , B_5^ε and B_6^ε are composed of terms without a 0-mode, and $E_n(s, t)$ is defined by

$$E_n(s, t) = \varepsilon \dot{R}_n(t) + (n^2 - 1)R_n(t) - \frac{e_n(s)}{2}.$$

Let $B_{i,n}^\varepsilon$ denote the n -th Fourier coefficient of B_i^ε for $i = 5, 6$. By projecting the equation onto each Fourier mode, we conclude that

$$(3.14) \quad \begin{cases} \dot{s} = \frac{4\varepsilon^2}{3\pi} K_s + \varepsilon B_{5,1}^\varepsilon \dot{s} + \varepsilon^3 B_{6,1}^\varepsilon, \\ \varepsilon^2 \dot{R}_0 = c'(v_c) w_\varepsilon(R_0) + \varepsilon C_2^\varepsilon, \\ \varepsilon \dot{R}_n = -(n^2 - 1)R_n + \frac{e_n}{2} + \varepsilon^{-1} B_{5,n}^\varepsilon \dot{s} + \varepsilon B_{6,n}^\varepsilon, \quad n \geq 2. \end{cases}$$

For the first equation, we solve for \dot{s} by collecting the terms and dividing by $1 - \varepsilon B_{5,1}^\varepsilon$. This reveals that $\dot{s} = O(\varepsilon^2)$. Furthermore, assuming that w_ε is of order ε^l with $l \geq 0$, and setting $w(R_0) = \varepsilon^{-l} w_\varepsilon(R_0)$, we arrive at the following system:

$$(3.15) \quad \begin{cases} \dot{s} = \frac{4\varepsilon^2}{3\pi} K_s + \varepsilon^3 \tilde{B}_{6,1}^\varepsilon, \\ \varepsilon^{2-l} \dot{R}_0 = c'(v_c) w(R_0) + \varepsilon^{1-l} C_2^\varepsilon, \\ \varepsilon \dot{R}_n = -(n^2 - 1)R_n + \frac{e_n}{2} + \varepsilon \tilde{B}_{6,n}^\varepsilon, \quad n \geq 2, \end{cases}$$

where $\tilde{B}_{6,n}^\varepsilon$ represents the remainder terms. Specifically, for $n = 1$, $\tilde{B}_{6,1}^\varepsilon$ accounts for the higher-order terms generated by the division by $1 - \varepsilon B_{5,1}^\varepsilon$. For $n \geq 2$, $\tilde{B}_{6,n}^\varepsilon$ incorporates the corrections resulting from the substitution of \dot{s} , which is of order ε^2 . The first equation of the system (3.15) indicates that the leading-order dynamics of the interface position $s(t)$ are governed by

$$\dot{s} = \frac{4\varepsilon^2}{3\pi} K_s.$$

This relationship provides a rigorous mathematical basis for the “shape-sensing”. It implies that the interface is not passive but actively seeks out geometric features; specifically, the polarized domain is attracted to protrusions (local curvature maxima) and repelled from indentations. This mechanism allows the cell to orient itself purely based on the geometry of its environment, without external chemical gradients.

Finally, we investigate the stability of the equilibria for the problem (3.15). Letting $R = (R_0, R_2, R_3, \dots)$ by abuse of notation, we establish the following theorem concerning the existence and stability of the stationary solutions to (3.15).

THEOREM 3.1. *Let s^0 be a non-degenerate critical point of the boundary curvature $K(s)$, i.e., $K_s(s^0) = 0$ and $K_{ss}(s^0) \neq 0$. Then, for sufficiently small $\varepsilon > 0$, there exists a unique equilibrium solution $(s^\varepsilon, R^\varepsilon)$ to the system (3.15) in a neighborhood of the unperturbed equilibrium (s^0, R^0) . Moreover, the linear stability of $(s^\varepsilon, R^\varepsilon)$ is determined by the local geometry of the boundary at s^0 :*

- (1) *If s^0 is a local maximum of $K(s)$ (i.e., $K_{ss}(s^0) < 0$), the equilibrium is asymptotically stable.*
- (2) *If s^0 is a local minimum of $K(s)$ (i.e., $K_{ss}(s^0) > 0$), the equilibrium is unstable.*

Proof. Let $P(s, R, \varepsilon)$ denote the vector field given by the right-hand side of the system (3.15), rescaled such that the leading-order terms are of $O(1)$. Namely, $P(s, R, \varepsilon) = (P_0, P_1, P_2, \dots)$ where

$$\begin{aligned} P_0(s, R, \varepsilon) &= \frac{4}{3\pi} K_s(s) + \varepsilon \tilde{B}_{6,1}^\varepsilon, \\ P_1(s, R, \varepsilon) &= c'(v_c) w(R_0) + \varepsilon^{1-l} C_2^\varepsilon, \\ P_2(s, R, \varepsilon) &= -(2^2 - 1) R_2 + \frac{e_2}{2} + \varepsilon \tilde{B}_{6,2}^\varepsilon, \\ &\vdots \\ P_n(s, R, \varepsilon) &= -(n^2 - 1) R_n + \frac{e_n}{2} + \varepsilon \tilde{B}_{6,n}^\varepsilon, \\ &\vdots \end{aligned}$$

An equilibrium (s^0, R^0) of the unperturbed system ($\varepsilon = 0$) is a solution to $P(s, R, 0) = 0$, which must satisfy

$$\begin{aligned} K_s(s^0) &= 0, \\ w(R_0^0) &= 0, \text{ i.e., } v_0(R_0^0) = v_c, \\ R_n^0 &= \frac{e_n(s^0)}{2(n^2 - 1)} = 0 \text{ for } n \geq 2. \end{aligned}$$

We now examine the unique existence and stability of an equilibrium for the perturbed system ($\varepsilon > 0$) near (s^0, R^0) . The Jacobian matrix of P with respect to (s, R) evaluated at $(s^0, R^0, 0)$ forms a lower triangular matrix:

$$\begin{pmatrix} \frac{4}{3\pi} K_{ss}(s^0) & 0 & 0 & \cdots & 0 & \cdots \\ 0 & c'(v_c) w'(R_0^0) & 0 & \cdots & 0 & \cdots \\ \frac{e'_2(s^0)}{2} & 0 & -3 & \cdots & 0 & \cdots \\ \vdots & \vdots & \vdots & \ddots & \vdots & \ddots \\ \frac{e'_n(s^0)}{2} & 0 & 0 & \cdots & -(n^2 - 1) & \cdots \\ \vdots & \vdots & \vdots & \ddots & \vdots & \ddots \end{pmatrix}.$$

The eigenvalues of the above matrix are given by the diagonal entries: $\frac{4}{3\pi} K_{ss}(s^0)$, $c'(v_c) w'(R_0^0)$, and $-(n^2 - 1)$ for $n \geq 2$. Since we have $c'(v_c) w'(R_0^0) < 0$ (see the definition of w and Subsection 3.3), the Implicit Function Theorem guarantees that if $K_{ss}(s^0) \neq 0$, a unique solution to $P(s, R, \varepsilon) = 0$ exists in a neighborhood of $(s, R) = (s^0, R^0)$ for sufficiently small $\varepsilon > 0$. Furthermore, the stability of this solution for $\varepsilon > 0$ is the same as that of (s^0, R^0) and is therefore determined by the sign of $K_{ss}(s^0)$. Namely, the equilibrium for $\varepsilon > 0$ is stable if $K_{ss}(s^0) < 0$, and is unstable if $K_{ss}(s^0) > 0$. \square

4. Concluding Remarks. In this paper, we have derived a free boundary problem approximating the front behavior of the wave-pinning model valid up to the $O(\varepsilon^{-1})$ timescale via matched asymptotics. Our results analytically corroborate the emergence of area-preserving mean curvature flow on the $O(\varepsilon^{-1})$ timescale, a behavior that has been suggested in previous studies. Furthermore, we demonstrated that the interface undergoes a slow drift along the domain boundary on the $O(\varepsilon^{-2})$ timescale, driven by the interaction between curvature flow and boundary geometry.

While these findings provide theoretical insights into the long-time behavior of the wave-pinning model, several mathematical challenges remain. A rigorous convergence analysis of the original system to the derived interface equations as $\varepsilon \downarrow 0$ is required. For such rigorous treatments of reaction-diffusion systems and their interfaces, see [18] and references therein. In Section 3, we utilized a scaling argument to justify the assumption that the first-order correction v_1 is of order ε^2 ; however, verifying this assumption requires examining the properties of the transmission problem for v_1 , which necessitates a more delicate argument. Verifying this assumption would likely require establishing L^∞ estimates for the transmission problem on the perturbed domain, which involves subtle regularity issues at the boundary contact points. While we leave this rigorous proof for future work, the consistency of our asymptotic results with numerical simulations strongly supports the validity of this scaling ansatz. In addition to these analytical challenges, the numerical treatment of the v_1 term presents significant difficulties.

These complexities associated with v_1 lead us to consider a simplified model in which the v_1 term is neglected. This simplified model retains a sufficient mechanism for wave-pinning. Consequently, this simplified model serves not only as a valid approximation of the full wave-pinning model but also as a minimal framework that distills its essence, providing a tractable mathematical description suitable for investigating long-time behaviors. Detailed analysis of this simplified model also remains an interesting subject for future research.

We discuss the implications of our results for understanding cell motility models, specifically the model proposed by Camley et al. [9]. Their model, which couples the wave-pinning reaction-diffusion system with phase-field mechanics, exhibits a transition between straight and rotating motion depending on parameter values. Camley et al. hypothesized that “shape sensing” inherent to the wave-pinning kinetics plays a crucial role in the mechanism of rotation. Our derivation of the drift effect toward high-curvature regions provides analytical validation for this hypothesis. In the context of rotating motion, the mechanism can be interpreted as a mismatch between mechanical and chemical stable states. While mechanical forces driven by protrusion tend to deform the cell into a bilaterally symmetric shape (typically symmetric about the short axis), the internal reaction-diffusion dynamics drives the Rho GT-Pase interface toward regions of higher curvature (i.e., the tips of the long axis), as shown in our $O(\varepsilon^{-2})$ analysis. This continuous breaking of symmetry likely induces the rotational behavior observed in numerical simulations. Conversely, the existence of straight motion presents a mathematically intriguing phenomenon. In a migrating cell, the polarity is typically localized at the leading edge, which corresponds to a region of relatively low curvature compared to the sides. According to our analysis, such a configuration should be unstable, as the interface naturally drifts toward higher curvature. The persistence of straight motion, therefore, suggests that the kinetics of the moving boundary (protrusion forces) exert a stabilizing effect that counteracts the geometric drift. In other words, the coupling with boundary mechanics stabilizes a configuration that is inherently unstable within the pure wave-pinning framework.

Unraveling the mathematical structure of this competition—specifically, proving the existence and bifurcation of straight versus rotating solutions in the coupled system—remains a challenging and significant subject for future research.

Ultimately, our analysis suggests that cell polarity is a robust phenomenon where geometry acts as a governing cue. By reducing the complex reaction-diffusion system to a set of geometric evolution laws, we provide a theoretical tool that can be used to predict cell behavior in engineered micro-environments, bridging the gap between mathematical theory and experimental cell biology.

Acknowledgments. This work was supported by JSPS KAKENHI Grant Numbers JP22K03425, JP22K18677, JP23H00086, JP24K16964, 25K00918.

REFERENCES

- [1] N. D. ALIKAKOS, P. W. BATES, X. CHEN, AND G. FUSCO, *Mullins-Sekerka motion of small droplets on a fixed boundary*, J. Geom. Anal., 10 (2000), pp. 575–596, <https://doi.org/10.1007/BF02921987>.
- [2] N. D. ALIKAKOS, X. CHEN, AND G. FUSCO, *Motion of a droplet by surface tension along the boundary*, Calc. Var. Partial Differential Equations, 11 (2000), pp. 233–305, <https://doi.org/10.1007/s005260000052>.
- [3] N. D. ALIKAKOS AND G. FUSCO, *Slow dynamics for the cahn-hilliard equation in higher space dimensions: the motion of bubbles*, Arch. Ration. Mech. Anal., 141 (1998), pp. 1–61, <https://doi.org/10.1007/s002050050072>.
- [4] S. J. ALTSCHULER, S. B. ANGENENT, Y. WANG, AND L. F. WU, *On the spontaneous emergence of cell polarity*, Nature, 454 (2008), pp. 886–889, <https://doi.org/10.1038/nature07119>.
- [5] D. M. BRYANT AND K. E. MOSTOV, *From cells to organs: building polarized tissue*, Nat. Rev. Mol. Cell Biol., 9 (2008), pp. 887–901, <https://doi.org/10.1038/nrm2523>.
- [6] M. T. BUTLER AND J. B. WALLINGFORD, *Planar cell polarity in development and disease*, Nat. Rev. Mol. Cell Biol., 18 (2017), pp. 375–388, <https://doi.org/10.1038/nrm.2017.11>.
- [7] G. CAGINALP AND P. C. FIFE, *Dynamics of layered interfaces arising from phase boundaries*, SIAM J. Appl. Math., 48 (1988), pp. 506–518, <https://doi.org/10.1137/0148029>.
- [8] B. A. CAMLEY, Y. ZHAO, B. LI, H. LEVINE, AND W.-J. RAPPEL, *Periodic migration in a physical model of cells on micropatterns*, Phys. Rev. Lett., 111 (2013), p. 158102, <https://doi.org/10.1103/PhysRevLett.111.158102>.
- [9] B. A. CAMLEY, Y. ZHAO, B. LI, H. LEVINE, AND W.-J. RAPPEL, *Crawling and turning in a minimal reaction-diffusion cell motility model: Coupling cell shape and biochemistry*, Phys. Rev. E, 95 (2017), p. 012401, <https://doi.org/10.1103/PhysRevE.95.012401>.
- [10] J. P. CAMPANALE, T. Y. SUN, AND D. J. MONTELL, *Development and dynamics of cell polarity at a glance*, J. Cell Sci., 130 (2017), pp. 1201–1207, <https://doi.org/10.1242/jcs.188599>.
- [11] R. DIEGMILLER, H. MONTANELLI, C. B. MURATOV, AND S. Y. SHVARTSMAN, *Spherical caps in cell polarization*, Biophys. J., 115 (2018), pp. 26–30, <https://doi.org/10.1016/j.bpj.2018.05.033>.
- [12] L. EDELSTEIN-KESHE, W. R. HOLMES, M. ZAJAC, AND M. DUTOT, *From simple to detailed models for cell polarization*, Philos. Trans. R. Soc. B Biol. Sci., 368 (2013), p. 20130003, <https://doi.org/10.1098/rstb.2013.0003>.
- [13] S.-I. EI, M. IIDA, AND E. YANAGIDA, *Dynamics of interfaces in a scalar parabolic equation with variable diffusion coefficients*, Japan J. Indust. Appl. Math., 14 (1997), pp. 1–23, <https://doi.org/10.1007/BF03167306>.
- [14] S.-I. EI AND E. YANAGIDA, *Slow dynamics of interfaces in the allen-cahn equation on a strip-like domain*, SIAM J. Math. Anal., 29 (1998), pp. 555–595, <https://doi.org/10.1137/S00361419096307205>.
- [15] G. FUSCO AND J. K. HALE, *Slow-motion manifolds, dormant instability, and singular perturbations*, J. Dynam. Differential Equations, 1 (1989), pp. 75–94, <https://doi.org/10.1007/BF01048791>.
- [16] W. GIESE, M. EIGEL, S. WESTERHEIDE, C. ENGWER, AND E. KLIPP, *Influence of cell shape, inhomogeneities and diffusion barriers in cell polarization models*, Phys. Biol., 12 (2015), p. 066014, <https://doi.org/10.1088/1478-3975/12/6/066014>.
- [17] N. W. GOEHRING, P. K. TRONG, J. S. BOIS, D. CHOWDHURY, E. M. NICOLA, A. A. HYMAN, AND S. W. GRILL, *Polarization of par proteins by advective triggering of a pattern-forming*

system, *Science*, 334 (2011), pp. 1137–1141, <https://doi.org/10.1126/science.1208619>.

[18] D. GOMEZ, K.-Y. LAM, AND Y. MORI, *Front propagation in the shadow wave-pinning model*, *J. Math. Biol.*, 86 (2023), p. 72, <https://doi.org/10.1007/s00285-023-01908-6>.

[19] A. B. GORYACHEV AND M. LEDA, *Many roads to symmetry breaking: molecular mechanisms and theoretical models of yeast cell polarity*, *Mol. Biol. Cell.*, 28 (2017), pp. 370–380, <https://doi.org/10.1091/mbc.E16-10-0739>.

[20] A. B. GORYACHEV AND A. V. POKHILKO, *Dynamics of cdc42 network embodies a turing-type mechanism of yeast cell polarity*, *FEBS Lett.*, 582 (2008), pp. 1437–1443, <https://doi.org/10.1016/j.febslet.2008.03.029>.

[21] W. R. HOLMES, A. E. CARLSSON, AND L. EDELSTEIN-KESHET, *Regimes of wave type patterning driven by refractory actin feedback: transition from static polarization to dynamic wave behaviour*, *Phys. Biol.*, 9 (2012), p. 046005, <https://doi.org/10.1088/1478-3975/9/4/046005>.

[22] A. JILKINE, *A wave-pinning mechanism for eukaryotic cell polarization based on Rho GTPase dynamics*, PhD thesis, University of British Columbia, Vancouver, BC, Canada, 2009.

[23] A. JILKINE AND L. EDELSTEIN-KESHET, *A comparison of mathematical models for polarization of single eukaryotic cells in response to guided cues*, *PLoS Comput. Biol.*, 7 (2011), p. e1001121, <https://doi.org/10.1371/journal.pcbi.1001121>.

[24] M. LEE AND V. VASIOUKHIN, *Cell polarity and cancer-cell and tissue polarity as a non-canonical tumor suppressor*, *J. Cell Sci.*, 121 (2008), pp. 1141–1150, <https://doi.org/10.1242/jcs.016634>.

[25] A. F. MARÉE, V. A. GRIENEISEN, AND L. EDELSTEIN-KESHET, *How cells integrate complex stimuli: the effect of feedback from phosphoinositides and cell shape on cell polarization and motility*, *PLoS Comput. Biol.*, 8 (2012), p. e1002402, <https://doi.org/10.1371/journal.pcbi.1002402>.

[26] P. W. MILLER, D. FORTUNATO, M. NOVAGA, S. Y. SHVARTSMAN, AND C. B. MURATOV, *Generation and motion of interfaces in a mass-conserving reaction-diffusion system*, *SIAM J. Appl. Dyn. Syst.*, 22 (2023), pp. 2408–2431, <https://doi.org/10.1137/22M152548X>.

[27] Y. MORI, A. JILKINE, AND L. EDELSTEIN-KESHET, *Wave-pinning and cell polarity from a bistable reaction-diffusion system*, *Biophys. J.*, 94 (2008), pp. 3684–3697, <https://doi.org/10.1529/biophysj.107.120824>.

[28] Y. MORI, A. JILKINE, AND L. EDELSTEIN-KESHET, *Asymptotic and bifurcation analysis of wave-pinning in a reaction-diffusion model for cell polarization*, *SIAM J. Appl. Math.*, 71 (2011), pp. 1401–1427, <https://doi.org/10.1137/10079118X>.

[29] K.-I. NAKAMURA, H. MATANO, D. HILHORST, AND R. SCHÄTZLE, *Singular limit of a reaction-diffusion equation with a spatially inhomogeneous reaction term*, *J. Statist. Phys.*, 95 (1999), pp. 1165–1185, <https://doi.org/10.1023/A:1004518904533>.

[30] M. OTSUJI, S. ISHIHARA, C. CO, K. KAIBUCHI, A. MOCHIZUKI, AND S. KURODA, *A mass conserved reaction-diffusion system captures properties of cell polarity*, *PLoS Comput. Biol.*, 3 (2007), pp. 1040–1054, <https://doi.org/10.1371/journal.pcbi.0030108>.

[31] A. RÄTZ AND M. RÖGER, *Turing instabilities in a mathematical model for signaling networks*, *J. Math. Biol.*, 65 (2012), pp. 1215–1244, <https://doi.org/10.1007/s00285-011-0495-4>.

[32] J. RUBINSTEIN, P. STERNBERG, AND J. B. KELLER, *Fast reaction, slow diffusion, and curve shortening*, *SIAM J. Appl. Math.*, 49 (1989), pp. 116–133, <https://doi.org/10.1137/0149007>.

[33] A. R. SINGH, T. LEADBETTER, AND B. A. CAMLEY, *Sensing the shape of a cell with reaction diffusion and energy minimization*, *Proc. Nat. Acad. Sci. USA*, 119 (2022), p. e2121302119, <https://doi.org/10.1073/pnas.2121302119>.

[34] B. VANDERLEI, J. J. FENG, AND L. EDELSTEIN-KESHET, *A computational model of cell polarization and motility coupling mechanics and biochemistry*, *Multiscale Model. Simul.*, 9 (2011), pp. 1420–1443, <https://doi.org/10.1137/100815335>.

[35] N. VERSCHUEREN AND A. CHAMPENEYS, *A model for cell polarization without mass conservation*, *SIAM J. Appl. Dyn. Syst.*, 16 (2017), pp. 1797–1830, <https://doi.org/10.1137/16M1093847>.

[36] A. WODARZ AND I. NÄTHKE, *Cell polarity in development and cancer*, *Nat. Cell Biol.*, 9 (2007), pp. 1016–1024, <https://doi.org/10.1038/ncb433>.

[37] C. ZMURCHOK, D. BHASKAR, AND L. EDELSTEIN-KESHET, *Coupling mechanical tension and gtpase signaling to generate cell and tissue dynamics*, *Phys. Biol.*, 15 (2018), p. 046004, <https://doi.org/10.1088/1478-3975/aab1c0>.